Chapter 6
Heterogeneity of Electrical Conductivity in the Oceanic Upper Mantle

Tomoo Katsura and Takashi Yoshino

Abstract We discuss conductivity heterogeneities of the oceanic upper mantle using available experimental data. The activation energy of the polaron conduction in olivine, wadsleyite, and ringwoodite is similar, at 1.4–1.6 eV. The ionic conduction is significant in olivine, but not in wadsleyite and ringwoodite. Its activation energy is much larger than that of the small polaron conduction (7–12 eV). The proton conductions have a smaller activation energy than the small polaron conduction (less than 1 eV) and are negligible at high temperatures in the depleted MORB mantle. The effects of the secondary minerals are negligible. No significant conductivity jump is associated with the olivine–wadsleyite transition. Volatile components greatly increase conductivity of basaltic melt. The anisotropy in both intrinsic and proton conditions in olivine is small. Sheared, partially molten peridotite can show conductivity anisotropy. The high conductivity below mid-oceanic ridges could be caused by partial melting. Conductivity at several locations suggests a melt fraction of the order of 0.1 vol.%, whereas that under the East Pacific Rise at 9°N suggests one of 15 vol.%. Lithosphere has low conductivity, which should be primarily due to its low temperature. However, the conductivity is too high, judging from the temperature structure and intrinsic conduction of olivine. The circulation of water does not provide enough explanation. The high-conductivity layer at the top of the asthenosphere is not a ubiquitous feature of the mantle—it is relatively limited to regions under young plates. The associated conductivity anisotropy suggests its partial melting origin. The conductivity in the mantle transition zone can be explained by the intrinsic conduction of wadsleyite and ringwoodite. Estimations of water content in the transition zone are largely affected by the uncertainty of geophysical modeling. The MT studies do not detect mantle

T. Katsura (✉)
Bayerisches Geoinstitut, University of Bayreuth, 95440 Bayreuth, Germany
e-mail: tomo.katsura@uni-bayreuth.de

T. Yoshino
Institute for Study of the Earth's Interior, Okayama University,
Misasa 612-0193, Japan

A. Khan and F. Deschamps (eds.), *The Earth's Heterogeneous Mantle*,
Springer Geophysics, DOI 10.1007/978-3-319-15627-9_6

plumes, although the seismic studies show the presence of low-velocity zones. The conductivity anomalies, whose origins are not understood, are observed under the southern Philippine Sea and the broad region north of Hawaii.

Keywords Electrical conductivity · Small polaron conduction · Ionic conduction · Proton conduction · Magnetotellurics · Olivine · Wadsleyite · Ringwoodite · Mantle heterogeneity

6.1 Introduction

Electrical conductivity is a physical parameter that can be estimated from the earth's surface by means of the magnetotelluric (MT) and geomagnetic deep soundings (GDS) method. Unfortunately, however, spatial resolutions of MT studies are by far worse than those of seismic studies (cf. Fukao et al. 2004). Additionally, although seismic studies can detect variation in elasticity of the order of 0.1 %, variation by factors is necessary to detect conductivity anomalies by the MT and GDS methods. Nevertheless, electrical conductivity can provide valuable information about the earth's depths.

Fortunately, conductivity of minerals can vary by orders of magnitude. One reason for the importance of conductivity studies is this large variation: A large variation in conductivity allows the detection of a conductive phase with a small volume fraction. Furthermore, some chemical variations that are difficult to detect with a seismic study can be detected: Those in defect structures and amounts of impurities produce conductivity variation, whereas those in chemical bonding between major constituent atoms could be caused by elastic variation. As Jacobsen (2006) suggested, although elastic moduli decrease with increasing water content at a given pressure, the effects of water on the elastic moduli become smaller with increasing pressure because of the larger pressure dependence of elastic moduli with the increasing water content. On the other hand, many workers reported that water incorporation in nominally anhydrous minerals largely increases their conductivity (cf. Yoshino and Katsura 2013). Thus, conductivity studies should provide different and independent information about the earth's interior to that from seismic studies.

Another point that we should mention is that regions that can be studied with electrical methods are different from those that can be seismically studied. The distribution of seismicity is quite heterogeneous in the earth, whereas the source signals of the MT and GDS observations are the variations in the electromagnetic field from space, available anywhere on earth. The electromagnetic waves from space penetrate the mantle vertically, allowing us to study conductivity structures under observatories. Seismic structures are obtained for the regions between observatories and large earthquakes.

In this article, we try to understand the conductivity variation in the oceanic upper mantle. Because the oceans cover 70 % of the earth's surface, the oceanic mantle

should be representative of the earth's mantle. We focus on the upper mantle and do not consider the lower mantle, although results of observational and experimental studies for the lower mantle conductivity recently exist (cf. Velimsky 2010; Ohta et al. 2010). We first review results of laboratory conductivity measurements to discuss possible reasons for the creation of conductivity heterogeneity in the mantle. We then discuss geophysical observations of conductivity heterogeneity in the oceanic upper mantle, using the experimental results discussed in the first part. Since the authors have been studying electrical conductivity of geomaterials (cf. Fuji-ta et al. 2004, 2007; Katsura et al. 1998, 2007; Manthilake et al. 2009; Yoshino and Katsura 2009, 2012, 2013; Yoshino et al. 2003, 2004, 2006, 2008a, b, c, 2009a, b, 2010, 2011; 2012a, b; Zhang et al. 2012, 2014), but are no MT and GDS experts, we have for the purposes of this article critically evaluated and selected experimental studies based on our experience. Of course, we are aware of a number of problems with MT and GDS studies, namely (1) strong model dependency (Shimizu et al. 2010a) and (2) the effects of surrounding geometry and conductivity structures (Heinson and Constable 1992). On the other hand, we have less MT and GDS study results that have been clearly disputed in literature.

Throughout this article, we assume that the mantle consists of two kinds of materials: the depleted MORB mantle (DMM) and the enriched mantle (EM). The DMM occupies the majority of the upper mantle, whereas the EM is associated with mantle plumes. As Workman et al. (2006) argued, the EM contains several times more volatile components than the DMM. According to Hirschmann (2010), we assume that the DMM contains 100 and 60 ppm of H_2O and CO_2, respectively, whereas the EM contains 300–900 and 120–1800 ppm of H_2O and CO_2, respectively.

6.2 Laboratory Conductivity Measurements of Upper Mantle Constituents

6.2.1 Mathematical Expression of Conductivity

Electrical conduction in the upper mantle minerals is a thermal activation process. For this reason, the temperature and pressure dependence of conductivity of minerals is assumed to follow the Arrhenius relation.

$$\sigma = \sigma_0 \exp\left[-\frac{H_a}{RT}\right] = \sigma_0 \exp\left[-\frac{E_a + PV_a}{RT}\right] \tag{6.1}$$

where σ_0 is the pre-exponential term, H_a is the activation enthalpy, E_a is the activation energy, V_a is the activation volume, R is the gas constant, T is the temperature, and P is the pressure. The pre-exponential term σ_0 expresses the population of charge. The activation energy E_a expresses the energy barrier for the charge transfer at ambient pressure—the large E_a means that conductivity rapidly decreases with decreasing temperature. The activation enthalpy H_a expresses the

high-pressure correction of E_a. The pressure dependence is considered to be linear with the constant activation volume V_a. The positive V_a means that conductivity has negative pressure dependence. Note that, although the population of charge could vary with pressure, it is usually assumed that only the energy barrier varies with pressure. The frequently used units of H_a, E_a, V_a, P, and T are kJ/mol, kJ/mol, cm^3, GPa, and K, respectively. The unit eV is also frequently used for E_a. In this case, the gas constant should be replaced by the Boltzmann constant k. If more than two mechanisms are considered to contribute to the bulk conductivity, the conductivity is expressed by the sum of Arrhenius equations.

Electrical conduction in liquid phases such as aqueous fluids, silicate melts, and carbonate melts is also a thermal activation process. Due to the complexity of electrical conduction in liquid phases, there is no widely accepted formula for the electrical conduction of liquid phases. In some studies, the obtained temperature dependence of electrical conductivity is well expressed using a single Arrhenius relation (Eq. 6.1) (cf. Waff and Tyburczy 1983; Gaillard 2004). Other studies find that the temperature dependence of conductivity largely deviates from the Arrhenius relations (cf. Ni et al. 2011). Ni et al. (2011) applied the Vogel–Tammann–Fulcher (VTF) equation (Angel and Smith 1982) originally developed to express the temperature dependence of viscosity in the expression of conductivity of liquid phases, because both electrical conduction and viscosity are related to the body motion of ions in liquid phases. The simple formula for the VTF equation is:

$$\sigma = A \exp\left[-\frac{B}{T - T_0}\right] \tag{6.2}$$

where A, B, and T_0 are empirical parameters. Conductivity in this expression decreases with decreasing temperature less strongly than in the Arrhenius equation, especially at lower temperatures.

6.2.2 Intrinsic Conduction of Olivine

Since olivine is the most abundant mineral in the upper mantle, its electrical properties have been studied extensively. Most efforts to understand the intrinsic conduction were made until 2000. Intrinsic conduction in this paper refers to electrical conduction by major chemical components. Since olivine is a ferromagnesian mineral, hopping of electron holes between ferrous and ferric iron, often called the small polaronconduction (cf. Wanamaker and Duba 1993), should be the most essential intrinsic conduction mechanism. Another mechanism is the migration of Mg vacancies, called ionic conduction in this chapter. Schock et al. (1989) demonstrated the importance of this mechanism at high temperatures. Separation of these two mechanisms is often difficult because ionic conduction becomes visible only in a small range of inverse temperatures in an Arrhenius plot. Therefore, we treat these two mechanisms as one intrinsic mechanism in most of this paper.

The following is a summary of properties of the intrinsic conduction in olivine.

1. Small polaron conduction is dominant up to 1500 K. Above this temperature, ionic conduction gradually becomes significant (Constable 2006).
2. The activation energy of small polaron conduction is about 1.5–1.7 eV (Constable and Duba 1990; Shankland and Duba 1990; Constable et al. 1992; Xu et al. 1998; Yoshino et al. 2009a, b). These values are smaller than the ionic conduction but larger than that of the proton conduction mentioned later. The small polaron conduction decreases significantly at low temperatures.
3. The activation energy of ionic conduction is very high. Due to difficulty in separating the ionic conduction from the small polaron conduction, its activation energy is not clear. However, it is reported to be from 7 to 12 eV (Constable et al. 1992; Constable and Duba 1990).
4. The absolute values of conductivity increase with increasing Fe content (decreasing Mg# = 100 Mg/(Mg + Fe)) at the same oxygen buffer (Omura et al. 1989; Yoshino et al. 2012). Although the degree of increase in conductivity with Fe content varies with temperature because of the Fe content dependence of activation energy mentioned below, conductivity of olivine with Mg# = 80 composition is half an order of magnitude higher than that with Mg# = 90 composition at upper mantle temperatures.
5. The activation energy decreases with increasing Fe content (decreasing Mg#) (Omura et al. 1989; Yoshino et al. 2012). The activation energy decreases by 0.2 eV when the Mg# changes from 90 to 80.
6. Conductivity increases proportionally to 0.18 the power of oxygen fugacity (Wanamaker and Duba 1993; Duba and Constable 1993). Namely, the oxidation state slightly affects conductivity.
7. Silica activity slightly affects conductivity. Wanamaker and Duba (1993) showed that a pyroxene-buffered sample has up to 0.2 log unit lower conductivity than a self-buffered sample.
8. Conductivity in the [001] direction is by a factor of about two higher than that in the [100] and [010] directions at temperatures of the upper mantle (Schock et al. 1989; Shankland and Duba 1990; Du Frane et al. 2005). Although the conductivity anisotropy in olivine is small, the degree of anisotropy increases with decreasing temperature.
9. Olivine conductivity has positive pressure dependence, namely negative activation volume (Yoshino et al. 2012b). The absolute values of activation volume decrease with increasing Mg#, and the pressure dependence of the intrinsic conduction of the mantle olivine is very small.

In this paper, we use the Constable's (2006) SO3 model as a reference for the intrinsic conductivity of mantle olivine with the assumption that the mantle oxygen fugacity is near the QFM buffer (Fig. 6.1).

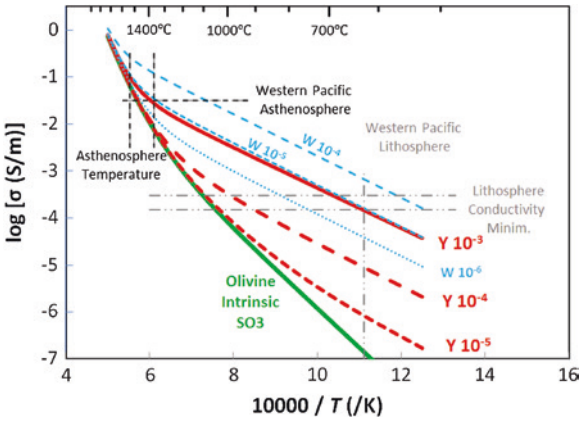

Fig. 6.1 Electrical conductivity of olivine. The *green curve* denotes a reference intrinsic conduction model of mantle olivine "SO3" proposed by (Constable (2006)). The *red* and *blue curves* denote the sum of the intrinsic and proton conduction with different water content, where the proton conduction is based on (Yoshino et al. (2009a, b) and Wang et al. (2006). The numbers next to these *curves* indicate the weight fraction of water in olivine, namely 10^{-3} or 0.1 wt% of water. The contribution of proton conduction is prominent at low temperatures but becomes negligible at temperatures corresponding to the asthenosphere. The two *vertical black broken lines* denote the range of temperature in the asthenosphere down to 400 km depth according to Katsura et al. (2010). The *horizontal black broken line* denotes conductivity of asthenosphere under the Western Pacific to the east of Izu Islands at 250–300 km depth reported by Baba et al. (2010). The *vertical gray line denotes* the possible temperature at a depth of 50 km in this region. The *horizontal gray broken lines* denote the minimum conductivity in this region

6.2.3 Proton Conduction of Olivine

Proton conduction is an electrical charge transfer by the migration of H^+. Since olivine can incorporate water under pressure in spite of its nominally anhydrous formula, the proton conduction could be significant as the dominant conduction mechanism in the deep mantle (Karato 1990). Subsequent to this finding, proton conduction has received attention from many scientists in this field (cf. Constable 1993; Evans et al. 1999; Baba 2005). Before proton conduction in olivine was actually measured, it was estimated using hydrogen diffusion data in olivine provided by Mackwell and Kohlstedt (1990) and Kohlstedt and Mackwell (1998). This estimation predicted more than one order of magnitude higher conductivity than the intrinsic conduction and more than one order of magnitude higher anisotropy (cf. Karato 1990; Evans et al. 2005).

In the late 2000s, three groups reported proton conduction of olivine (Wang et al. 2006; Yoshino et al. 2006, 2009a, b; Poe et al. 2010). Although the results of Poe et al. (2010) agree with those of Yoshino et al. (2009a, b) at relatively low water contents, Wang et al. (2006) report significantly higher proton conduction at the same water content than those of the other two groups. There are a few indicators of the reliability of the Yoshino et al. (2009a, b) results. Firstly, Yoshino et al.

(2006), (2009a, b) and Yoshino and Katsura (2012) demonstrated that water in doped olivine is released at temperatures above 1000 K. Above 1000 K, olivine conductivity is masked by a fluid phase and therefore, it is impossible to measure the conductivity of anhydrous olivine. Nevertheless, Wang et al. (2006) measured conductivity at temperatures up to 1273 K. Secondly, Yoshino et al. (2006) observed changes in conductivity, with water content down to the conditions where the effects of proton conduction are almost masked by the intrinsic conduction. Wang et al. (2006) measured proton conduction only when conductivity is more than one order of magnitude higher than the supposed intrinsic conduction. This group has actually never shown measurements of the intrinsic conduction of olivine. Thirdly, the impedance spectra produced by Yoshino et al. (2009a, b) showed almost perfect semi-arcs with a tail, which indicates that only one conduction mechanism is responsible for conductivity, although there is some reaction with the electrode. Although Wang et al. (2006) did not show any impedance spectra, impedance spectra of water-doped, nominally anhydrous minerals given by this group usually show strong distortion, further discussed by Yoshino and Katsura (2012). Since Yoshino and Katsura (2013) discussed all these points in detail, the proton conduction in olivine discussed in this article is based on Yoshino et al. (2006, 2009a, b) .

The following are summaries of the proton conductivity of olivine from Yoshino et al. (2006, 2009a, b).

1. Proton conduction increases with increasing water content. Although there is an additional effect on the activation energy mentioned below, the magnitude of proton conduction is essentially proportional to the water content.
2. The activation energy decreases with increasing water content, linearly with one-third power of water content: $\sigma_{\mathrm{p}} = \sigma_{\mathrm{p}_0} \exp\left[-\frac{E_0 - \alpha C_{\mathrm{H_2O}}^{1/3}}{kT}\right]$, where σ_{p} is the proton conduction, σ_{p_0} is the pre-exponential term of the proton conduction, E_{P_0} is the activation energy of the proton conduction at zero water, $C_{\mathrm{H_2O}}$ is the water content, k is the Boltzmann factor, T is the absolute temperature, and α is the constant. The activation energy of the proton conduction at zero water is $E_{\mathrm{P}_0} = 0.92$ eV. Thus, the activation energies of proton conduction are lower than those of intrinsic conduction (1.4–12 eV). Consequently, proton conduction dominates at low temperatures. At asthenospheric temperatures, the contribution of proton conduction is very small.
3. Although a large anisotropy is expected from the hydrogen diffusion data (cf. Evans et al. 2005), the proton conduction in olivine is essentially isotropic at asthenospheric temperatures (Yoshino et al. 2006; Yang 2012) (Fig. 6.2). The anisotropy of proton conduction is actually even smaller than that of the intrinsic conduction. Although the hydrogen diffusion experiments (Mackwell and Kohlstedt 1990; Kohlstedt and Mackwell 1998) did not report a decrease in anisotropy with increasing temperature, this is due to their large experimental uncertainty.
4. There is no report about the activation volume of proton conduction of olivine. Since the ionic volume of protons is small, the pressure effect on proton conduction should be small, i.e., the activation energy is nearly zero.

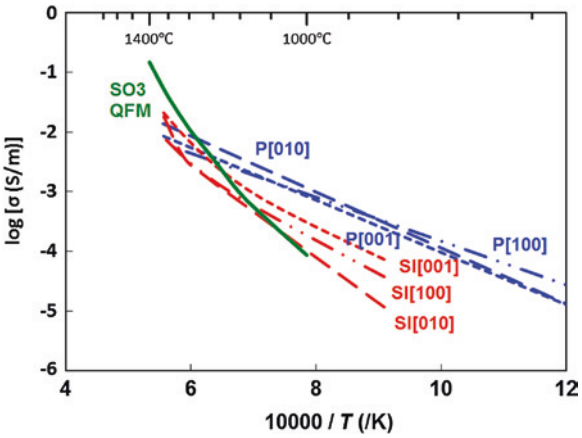

Fig. 6.2 Conductivity anisotropy of the intrinsic (SI, *red*) and proton (P, *blue*) conductions of olivine. The original data are from Constable et al. (1992) (intrinsic conduction) and Yoshino et al. (2006) (proton conduction). The anisotropy in proton conduction is negligible at high temperatures between 1000 and 1700 K and even smaller than that in intrinsic conduction

In comparison, the following are summaries of proton conduction from Wang et al. (2006) (Fig. 6.1).

1. Proton conduction increases proportionally to the power of 0.62 of the water content.
2. The activation energy is independent of water content and is 0.92 eV.
3. The magnitudes of the proton conductions are about two orders of magnitude higher than those reported by Yoshino et al. (2006).

6.2.4 Olivine High-Pressure Polymorphs

Olivine transforms to wadsleyite and then to ringwoodite in the upper mantle. The conductivity of wadsleyite and ringwoodite has been studied extensively compared to olivine because their conductivity is thought to govern the conductivity of the transition zone (cf. Yoshino and Katsura 2013). Since wadsleyite and ringwoodite incorporate even higher amounts of water than olivine (Keppler and Bolfan-Casanova 2006), the proton conduction of these minerals was considered to be important in understanding the transition zone conductivity as well as the intrinsic conductivity. We note that there are huge discrepancies in the magnitude of proton conduction of wadsleyite and ringwoodite, as well as that of olivine, among different data sets (Huang et al. 2005; Yoshino et al. 2008a, b, c; Dai and Karato 2009; Karato and Dai 2009; Romano et al. 2009; Yoshino and Katsura 2009, 2013). Although the conclusion is still indefinite, we will adopt the results from Yoshino et al. (2008a, b, c), Manthilake et al. (2009), and Yoshino and Katsura (2012) in the present chapter, as explained in Yoshino and Katsura (2013).

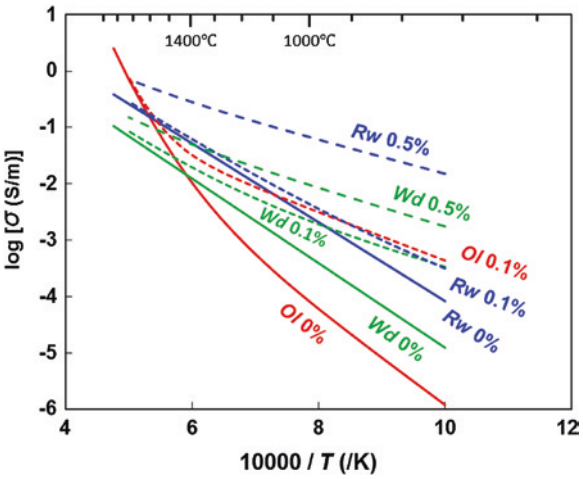

Fig. 6.3 Comparison of the intrinsic and total (intrinsic + proton) conductions of olivine (*red*), wadsleyite (*green*), and ringwoodite (*blue*). The *solid*, *short-broken,* and *long-broken curves* denote conductivity of these minerals with water contents of 0, 0.1, and 0.5 wt%. The original data are from Yoshino et al. (2008a, b, c, 2009a, b). The intrinsic conduction increases with the high-pressure phase transition from olivine to wadsleyite and then to ringwoodite. The differences in conductivity among the three phases become smaller with the incorporation of 0.1 % of water. The contribution of the proton conduction of ringwoodite becomes significant above this water content

The following is a summary of the conductivity of wadsleyite and ringwoodite (Fig. 6.3).

1. The conductivity of these minerals without water increases with increasing iron content (Yoshino and Katsura 2009; Yoshino et al. 2012b). Therefore, the small polaronconduction should be the essential conduction mechanism.
2. There is no clear evidence for dominance of ionic conduction at high temperatures (cf. Xu et al. 1998; Yoshino et al. 2008a, b, c).
3. The activation energy of the small polaron conduction of wadsleyite and ringwoodite is similar to or slightly smaller than that of olivine, namely 1.5 and 1.4 eV, respectively (Yoshino and Katsura 2013).
4. The small polaron conductivity of wadsleyite is by 0.5 log unit higher than that of olivine. That of ringwoodite is by 0.7 log unit higher than that of wadsleyite (Yoshino and Katsura 2013).
5. Due to ionic conduction in olivine but not in wadsleyite and ringwoodite, the intrinsic conductivity of wadsleyite and ringwoodite is smaller than that of olivine at temperatures in the asthenosphere and transition zone (see the "*Ol* 0 %" curve in Fig. 6.3).
6. The magnitude of proton conduction in ringwoodite is much larger than that in olivine and wadsleyite. That in wadsleyite is slightly lower than that in olivine (Yoshino and Katsura 2013).
7. The activation energy of proton conduction in wadsleyite and ringwoodite decreases with increasing water content, linearly with one-third power of water

content as in olivine: $\sigma_p = \sigma_{p_0} \exp\left[-\frac{E_0 - \alpha C_{H_2O}^{1/3}}{kT}\right]$. The α values of olivine and wadsleyite are similar (0.16 and 0.20, respectively) but that of ringwoodite is 3 times larger (0.67).

8. As is assumed for olivine, the pressure effects on conduction should be negligible. Additionally, the stability fields of wadsleyite and ringwoodite are very narrow in pressure; therefore, their activation volumes do not have significance in terms of geophysics.

Following are summaries of proton conduction from Huang et al. (2005) and Dai and Karato (2009). The general tendencies to discrepancies in wadsleyite and ringwoodite are similar to those in olivine between Yoshino et al. (2009a, b) and Wang et al. (2006).

1. Proton conduction increases proportionally to the power of 0.7 of the water content.
2. The activation energyis independent of water content and is 0.90 and 0.67 eV in wadsleyite and ringwoodite, respectively.
3. The magnitudes of the proton conductions are about two orders of magnitude higher than those reported by Yoshino et al. (2006).

Figure 6.3 shows total conduction of olivine with 0 and 0.1 % of water, and wadsleyite and ringwoodite with 0, 0.1, and 0.5 % of water. Since ionic conduction is significant in olivine but not in wadsleyite and ringwoodite, the intrinsic conductivity of olivine exceeds that of wadsleyite at the temperature at 410 km depth (1810 ± 20 K) in the present model. It is not clear whether this feature is the real case or not. Many studies measured intrinsic conductivity of wadsleyite only up to 1470 K (Xu et al. 1998; Dai and Karato 2009), which cannot provide any information about the ionic conduction. Yoshino and Katsura (2012) measured wadsleyite conductivity up to 2000 K, and their data show some possible contribution by ionic conduction. The number of data points in this paper is, however, insufficient to estimate the contribution by ionic conduction by numerically separating it from the small polaron conduction. A detailed conductivity measurement for wadsleyite at even higher temperature is necessary to understand the ionic conduction of wadsleyite.

After Xu et al. (1998) claimed a large conductivity jump associated with the olivine–wadsleyite transition, some geophysical studies artificially set a conductivity jump at 400 km depth by releasing the smoothing conditions (cf. Utada et al. 2003). However, as Huang et al. (2005) later demonstrated, the wadsleyite sample of Xu et al. (1998) contained 0.07 % of water, and therefore, their data cannot be used to discuss the intrinsic conduction of wadsleyite. Hence, it is unnecessary to assume a large conductivity jump at a depth of 400 km in MT modeling based on the current experimental data.

6.2.5 Secondary Minerals

Olivine is not the only constituent mineral in the upper mantle. Garnet, Ca-rich pyroxene, and Ca-poor pyroxene are also petrologically important constituent

minerals. Their conductivity has been measured less extensively than olivine, and the reliability of the measurement is not high. One reason for the confusing results is their complex compositions. In the case of olivine, we can reasonably approximate its composition by a binary solution Mg_2SiO_4–Fe_2SiO_4. On the other hand, at least four components, e.g., $MgSiO_3$–$FeSiO_3$–$CaSiO_3$–Al_2O_3, are necessary to describe the compositions of pyroxene and garnet. They can also contain large amounts of ferric iron. Accordingly, their conductivity should vary largely with a Fe^{3+}/Fe^{2+} ratio. Although some efforts have been made to estimate the bulk rock conductivity from each mineral conductivity based on the Hashin–Shtrikman bounds, there is no experimental data showing that secondary minerals affect the bulk rock conductivity of peridotite (cf. Jones et al. 2009). Actually, Duba and Constable (1993) report that the conductivity of lherzolite with 65 % of olivine modal composition is identical to that of olivine. Olivine forms a network of conductivity in peridotite, which masks the effects of other minerals. The effect of these minerals on the bulk conductivity in the mantle should therefore be negligible. Hence, we ignore the effects of the other minerals on mantle conductivity in this paper.

6.2.6 Liquid Phases

In contrast to the secondary solid minerals, liquid phases could affect whole-rock conductivity. Waff and Bulau (1979) showed dihedral angles of 30–50° for the basalt–olivine systems. Yoshino et al. (2009a, b) reported that dihedral angles in the forsterite–H_2O system decrease with pressure and become zero above 7 GPa. These reports suggest that liquid phases form an interconnected network in the deep upper mantle even though their fractions are small. Moreover, the surface energy at grain edges formed by three minerals must be higher than that of grain surfaces formed by two minerals. Therefore, it is expected that liquid phases, even if their amounts are trace, should affect conductivity paths in the peridotite matrix.

The primary candidate for a liquid phase in the upper mantle is basaltic melt. Some studies measure electrical conductivity of basaltic melt (cf. Tyburczy and Waff 1983; Ni et al. 2011) (Fig. 6.3). The results suggest that the conductivity of dry basaltic melt is 0.5–0.9 log S/m at the temperature at the top of the oceanic asthenosphere (Fig. 6.4) and slightly increases with increasing temperature. The conductivity slightly decreases with increasing pressure up to 0.5–1.5 GPa, but it becomes almost constant above 1.5 GPa (Tyburczy and Waff 1983). Conductivity of dry basaltic melt is higher than that of the intrinsic conduction of olivine by about three orders of magnitude. Therefore, when the basaltic melt fraction is more than 1 %, the bulk conductivity is primarily a function of conductivity and the fraction of basaltic melt. Yoshino et al. (2010) studied the logarithmic relations between the bulk conductivity and basaltic melt fraction and obtained a basaltic melt fraction exponent of 0.89 (Fig. 6.5). Thus, the bulk conductivity is approximately proportional to the basaltic melt fraction.

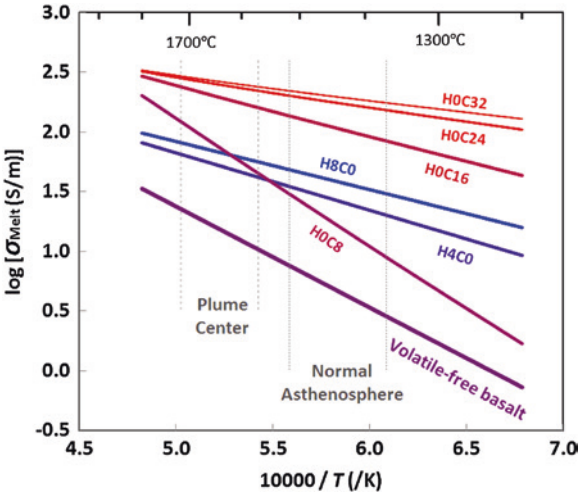

Fig. 6.4 Conductivity of basaltic melt with various H_2O and CO_2 contents by Sifre et al. (2014). The marking letters "H_C_" denote H_2O and CO_2 contents in the melt: The numbers after H and C indicate H_2O and CO_2 contents in wt%. The two pairs of *vertical bracketing lines* denote the temperature ranges of the normal asthenosphere based on Katsura et al. (2010) and the plume center based on the seismic wave anomalies reported by Montelli et al. (2006), and the relations between the temperature and shear-wave velocity reported by Faul (1997)

Recently, some groups studied conductivity anisotropy caused by small amounts of basaltic melt under shear (Caricchi et al. 2011; Zhang et al. 2014). Caricchi et al. (2011) measured the conductivity of natural peridotite with 4 or 8 % of basaltic melt in a torsion experiment. They found that the bulk conductivity normal to the shear is smaller than that under static conditions by one order of magnitude. Zhang et al. (2014) measured the conductivity of natural and model peridotite with 2 % of basaltic melt in the normal and parallel to shear on a shear plane simultaneously. They reported that the bulk conductivity in the normal and parallel shear directions is equivalent in the beginning of shear deformation, whereas that in the shear direction increased by one order of magnitude with increasing shear strain. Micro-texture analysis demonstrated that melt tubes were aligned in the shear direction, which should account for the high bulk conductivity in the shear direction. Since anisotropy of olivine does not cause conductivity anisotropy by more than a factor of three as previously mentioned, high-conductivity anisotropy should indicate the presence of a small fraction of liquid phases (Fig. 6.6).

H_2O is the most important volatile component in the upper mantle. Gaillard (2004) observed that conductivity of silicate melt (obsidian) increases in association with the addition of water. Ni et al. (2011) measured the conductivity of hydrous basaltic melt as a function of temperature and water content (Fig. 6.4). Hirschmann (2010) suggested that water content in the basaltic melt in the DMM and EM could be up to 2 and 6 wt%, respectively, at low degree of partial melting.

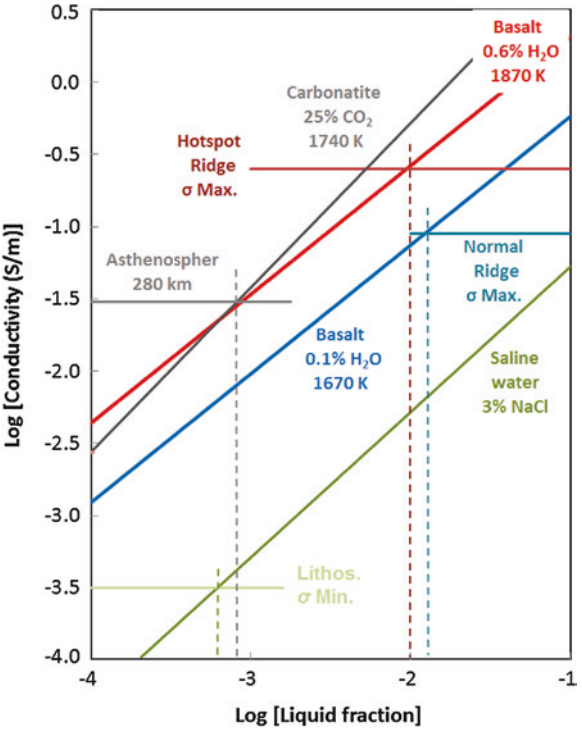

Fig. 6.5 Bulk conductivity of rocks against the fractions of liquid phases. *Green* saline water with 3 % of NaCl in quartzite (Shimojuku et al. 2014). *Blue* basalt with 0.1 % of H_2O in peridotite at 1670 K. *Red* basalt with 0.6 % of H_2O in peridotite at 1870 K based on the conductivity of hydrous basalt by Ni et al. (2011) and melt fraction exponent by Yoshino et al. (2010). *Gray* carbonatite with 25 % of CO_2 at 1740 K (Yoshino et al. 2010). The *dashed lines* denote the estimated fractions of the liquid phases at various tectonic settings

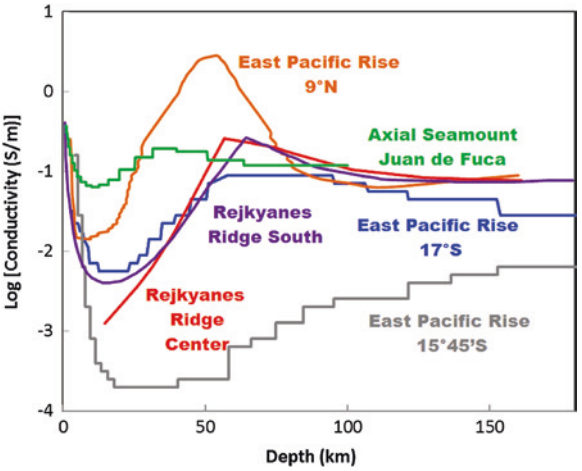

Fig. 6.6 One-dimensional conductivity beneath mid-oceanic ridges. *Blue and Gray* East Pacific Rise at 17°S and 15°45'S, respectively (Baba et al. 2006a, b). *Red* and *violet* Reykyanes Ridge (Heinson et al. 2000). *Green* Axial Seamount on the Juan de Fuca Ridge (Heinson et al. 1996). The intrinsic conductivity of olivine is in the order of 10^{-4} S/m and below the conductivity range shown in this figure

The 6 wt% of water increases the conductivity of basaltic melt by one order of magnitude.

CO_2 is another important volatile component in the mantle. Gaillard et al. (2008) demonstrated that molten carbonate has a conductivity of more than

3×10^2 S/m, which is by 2.5–3.5 orders of magnitude higher than that of basaltic melt. Sifre et al. (2014) modeled the effects of CO_2 and H_2O on the conductivity of basaltic melt by assuming the compensation law (Tyburczy and Waff 1983) and parallel conductive processes of hydrous basaltic melt and carbonate (Fig. 6.4). The effects of H_2O are large at low water content, but saturated at high water contents. The effects of CO_2 are smaller than H_2O below 10 wt%. However, they become significant at a CO_2 content above 8 %, exceeding the effects of water. These effects also seem saturated above 20 wt%. Proton can be incorporated in olivine and pyroxene, whereas carbon cannot be incorporated in silicate minerals. Consequently, the CO_2 content in the incipient melts can reach about 50 %, whereas that of H_2O should be limited to up to 7 % (Sifre et al. 2014). Therefore, the effects of CO_2 are more significant than those of H_2O in the majority of the asthenosphere, where the degree of partial melting should be less than 0.3 % (Hirschmann 2010). The relation of the bulk conductivity to the carbonatite melt fraction was studied by Yoshino et al. (2010), who reported a melt fraction exponent of 1.12 (Fig. 6.5).

Aqueous fluids are another possible liquid phase in the earth. However, silicate melts and fluid phases become miscible at high pressures. Mibe et al. (2011) demonstrated that the second critical point of the basalt + H_2O system is located at 3.4 GPa and 1100 K (Fig. 6.5). Therefore, no aqueous fluid phase is present below 100 km depth. In addition, the miscibility gap between a fluid phase and silicate melt should close at higher temperatures even at lower pressures. Mibe et al. (2011) observed that the miscibility gap closes at a temperature of 1600 K at a pressure of 1.8 GPa. Therefore, conductivity of fluid phases is important only at shallower parts of the mantle.

Although there is no measurement for the conductivity of aqueous fluid coexisting with peridotite, Shimojuku et al. (2014) measured the conductivity of brine-bearing quartzite at temperatures of 800–1100 K and a pressure of 1 GPa. They showed that the fluid conductivity is almost independent of temperature and the bulk rock conductivity increases with increasing salinity and fluid fraction. The bulk rock conductivity with a fluid phase with a constant salinity near that of seawater (3 wt%) is shown in Fig. 6.4.

6.3 Conductivity Heterogeneity in the Upper Mantle

6.3.1 High Conductivity Below Mid-Oceanic Ridges

Large amounts of basalt erupt at mid-oceanic ridges and huge partial melting regions are therefore expected under mid-oceanic ridges. Forsyth et al. (1998) estimated a minimum melt of 1–2 % down to 100 km depth under the East Pacific Rise,based on the seismic low-velocity anomaly. It is therefore expected that mid-oceanic ridge magmatism should cause a high-conductivity anomaly under ridges. There have actually been a number of reports on high-conductivity regions

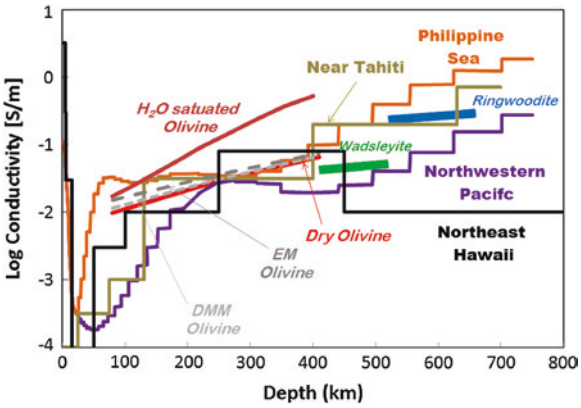

Fig. 6.7 One-dimensional conductivity structures under the Philippine Sea (*orange*) (Baba et al. 2010) and the northwestern Pacific near the Izu Islands (*violet*) (Baba et al. 2010) and near Tahiti (*olive*) (Nolasco et al. 1998). The conductivity of olivine under dry and water-saturated conditions is shown in *red* and *brown*. The conductivity of olivine with the DMM and EM compositions is denoted by *broken curves* in *dark* and *light gray,* respectively. The conductivity of dry wadsleyite and ringwoodite is shown in *green* and *blue*

under mid-oceanic ridges (Heinson and Lilley 1993; Heinson et al. 1993, 1996, 2000; Constable et al. 1997; Sinha et al. 1997; Evans et al. 1999, 2005; Baba et al. 2006a, b; Key et al. 2013) (Fig. 6.7).

Baba et al. (2006a) studied the two-dimensional conductivity structure under the East Pacific Rise at 17°S and showed a high-conductivity region of 9×10^{-2} S/m, 40 km in width, and vertically elongated from 50 to 120 km in depth immediately beneath the ridge axis. On the other hand, Baba et al. (2006b) showed no high-conductivity region under the East Pacific Rise at 15° 45′S: The conductivity at 50–80 km depth just beneath the axis is about 1–3 $\times 10^{-3}$ S/m. Key et al. (2013) illustrated the very detailed conductivity structure under the East Pacific Rise at 9°N. Their model shows that conductivity at the center of the high-conductivity region reaches 2 S/m. The regions with conductivity up to 2×10^{-1} S/m extend vertically from 20 to 80 km in depth and horizontally over 60 km. Thus, the presence of high-conductivity regions is very heterogeneous, even beneath the same ridge, the East Pacific Rise.

The adiabatic temperature at 50–80 km depth is about 1630–1680 K (Katsura et al. 2010). The intrinsic olivine conductivity is 3–5 $\times 10^{-3}$ S/m at these temperatures. These values explain conductivity beneath the East Pacific Rise at 15° 45′S but are far lower than the observed values at 17°S and 9°N. Therefore, the high conductivity at these regions should be explained by the MORB magmatism. The N-MORB (normal MORB) contains about 0.1 % of H_2O (cf. Sobolev and Chaussidon 1996), and such basaltic melt should have a conductivity of 20 S/m. Conductivities of 9×10^{-2} and 2 S/m suggest 0.2 and 10 vol.% of melt fractions beneath the East Pacific Rise at 17°S and 9°N, respectively, based on the melt fraction exponent of 0.89 for basaltic melt from Yoshino et al. (2010) (Fig. 6.4).

This melt fraction of 15 vol.% exceeds the threshold fraction for melt segregation (2–3 vol.%) (Faul 1997). The melt should be successively supplied and rise in this region. On the other hand, Forthys et al. (1998) estimate the melt fraction at 17°S to be 1–2 vol.%. Thus, the melt fraction based on the conductivity is much lower than that based on the seismic velocity anomaly.

Heinson et al. (1996) presented a one-dimensional conductivity structure under Axial Seamount on the Juan de Fuca Ridge. They showed a conductivity maximum of 2×10^{-1} S/m at a depth of 30–40 km. Heinson et al. (2000) studied the conductivity structures under the spreading center of the Reykjanes Ridge, the northern section of the mid-Atlantic Ridge. They showed conductivity maximum of 3×10^{-1} S/m at a depth of 60 km. These locations are known as the overlap of the ridge and a hot spot. As previously mentioned, the EM contains much higher volatile components than the DMM. Hung et al. (2004) studied the seismic structures beneath Iceland. From the velocity anomalies, they estimated that the temperature anomaly in this region is 150–200 K higher than the surrounding mantle. Nicholas et al. (2002) reported that the H_2O content in basaltic melt from the Reykjanes Ridge is up to 0.6 wt%. Such high water content would increase the melt conductivity, which should be enhanced by these high temperatures and high-volatile contents, and is estimated to be 40–60 S/m. From these values, the melt fraction is estimated to be 0.5–1 vol.%.

6.3.2 Lithosphere

As mentioned earlier on, the conductivity of minerals and liquids is a thermally activated process, and the mantle should have low conductivity at low-temperature regions. We emphasize that the Arrhenius relation (6.1) indicates that the magnitude of the conductivity anomaly by a low-temperature anomaly is more significant than that by a high-temperature one, if the magnitudes of the temperature anomalies are comparable.

Conductivity models under oceans depict low-conductivity layers at shallow regions. For example, Baba et al. (2010) showed conductivity minimums of 3×10^{-4} and 1.5×10^{-4} S/m at 20 and 50 km depth under the northern Philippine Sea and the Pacific Ocean to the east of the Izu Islands (Fig. 6.7). Conductivity in these regions monotonically increases with increasing depth below these depths. The Philippine Sea plate was formed 60 million years ago, and the Western Pacific plate of the studied area formed 125–150 million years ago. The temperatures at 20 and 50 km depth under the Philippine Sea and Western Pacific plates can be estimated at 600–1100 K and 900 K, respectively, based on the cooling model of the ocean plates. If the intrinsic conduction of olivine is the dominant conduction mechanism in such regions, the olivine conductivity should be lower than 1×10^{-5} S/m (Fig. 6.1). Therefore, the observed values are by more than one order of magnitude higher than expected from the intrinsic conductivity of olivine. Heinson and Constable (1992) had already indicated

that the observed conductivity in the lithosphere is significantly higher than that expected from the intrinsic conductivity of olivine. They argued that such discrepancy could be due to overestimation by geophysical modeling because of the coastal effect, for example.

Should a more conductive lithosphere than expected from the intrinsic conductivity of olivine not be due to analysis problems in geophysical modeling, it could be caused by proton conduction. However, proton conduction also has positive temperature dependence. In order to produce proton conduction of 1×10^{-4} S/m at 1000 K, about 1000 ppm of water is necessary, according to data from Yoshino et al. (2009a, b) (Fig. 6.1). However, the solubility of water at 1 GPa (30 km depth) is 100–200 ppm (cf. Keppler and Bolfan-Casanova 2006). Thus, proton conduction is insufficient for explaining the magnitude of the lithospheric conductivity.

Heinson and Constable (1992) argue that high conductivity at the shallowest depth could reflect circulation of saline water and the decrease in conductivity with depth in spite of a temperature increase should be due to crack closure with increased lithostatic pressure. By assuming the comparable salinity with seawater (3 %), the conductivity of 1–3 $\times$ 10^{-4} S/m can be achieved with 0.02–0.03 vol.% of the fluid phase (Fig. 6.5). However, the conductivity increases from the minimum 20 and 50 km depth to the deeper regions (Baba et al. 2010) which cannot be explained by this hypothesis because the conductivity of saline water is almost independent of temperature and a fluid fraction increase with increasing depth can hardly be considered.

6.3.3 Asthenosphere

Several studies in the 1970s and 1980s (cf. Larsen 1975; Filloux 1977; Oldenburg 1981) report "high-conductivity layers" in the oceanic asthenosphere. "High-conductivity layer" here is defined as a horizontal layer with maximum conductivity in the vertical direction. Since temperatures increase with increasing depth in the upper mantle, except for subduction zones, and conductivities of mantle minerals have positive temperature dependence but negligible pressure dependence, we specifically need to account for the high-conductivity layer. Heinson and Constable (1992), however, re-examined Oldenburg's (1981) analysis and concluded that the presence of the high-conductivity layer proposed by this study could be true but not robust enough. In addition, the majority of reported high conductivity in the oceanic asthenosphere should originate in the mid-oceanic ridge magmatism discussed above.

Nevertheless, we currently have examples showing high-conductivity layers at the top of the asthenosphere. Baba et al. (2006a) studied the conductivity structure in the region 150 km west to 350 km east of the East Pacific Rise at 17°S, down to 200 km depth, and defined a high-conductivity layer with a maximum of 9×10^{-2} S/m from 50 to 350 km east at 70–120 km depth (Fig. 6.8). Baba et al. (2006a)

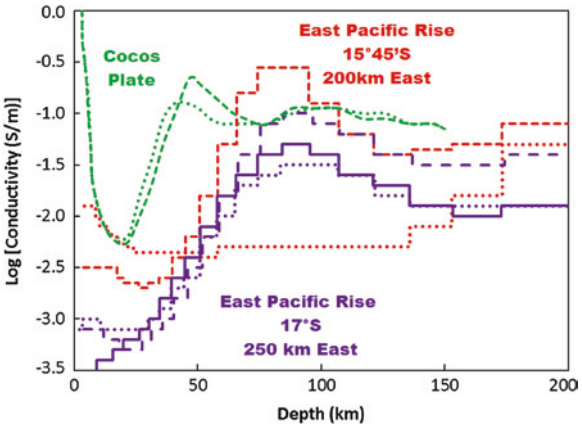

Fig. 6.8 The conductivity structures at the top of the asthenosphere under young plates. *Violet* East Pacific Rise at 17°S (Baba et al. 2006a). *Red* East Pacific Rise at 15° 45′S (Baba et al. 2006b). *Green* Cocos plate (Naif et al. 2013). The *solid line* denotes an isotropic structure. The *broken* and *dotted lines* denote anisotropic conductivity structures in the direction parallel and normal to the plate motion, respectively

and Evans et al. (2005) reported conductivity anisotropy in this high-conductivity layer, in which conductivity is by one order of magnitude higher in the direction parallel to the plate motion than in the normal direction. Naif et al. (2013) showed a conductivity structure in the 23–24-million-year-old region of the Cocos plate down to 150 km depth. They presented an anisotropic conductivity model with a maximum conductivity of 2×10^{-1} S/m at 50 km depth in the direction of the plate motion but almost no maximum in the other direction. Baba et al. (2006b) also illustrated an anisotropic conductivity model near the East Pacific Rise at 15° 45′S showing a high-conductivity layer of 3×10^{-1} S/m from 100 km east of the East Pacific Rise at 80–100 km depth in the direction of the plate motion. Although these regions are located near mid-oceanic ridges, Baba et al. (2010) studied conductivity structure under the northern Philippine Sea at depths down to 750 km. The conductivity in this region increases largely to reach 3×10^{-2} S/m from 20 to 70 km depth and slightly decreases by at most 1×10^{-2} S/m at 120 km depth (Fig. 6.7).

Nolasco et al. (1998) reported the conductivity structure under Tahiti, whose lithospheric age is 70 million years (Fig. 6.7). Their profile starts to increase from 1×10^{-4} S/m at the surface to 3×10^{-2} S/m at 130 km depth. The conductivity stays constant from this depth to 400 km depth. Thus, there is no high-conductivity layer in this region. Lizarralde et al. (1995) studied a conductivity structure between Hawaiiand California at depths from 150 to 1000 km. Their model reveals a conductive zone (0.05–0.1 S/m) between 250 and 450 km depth and a positive gradient in regions deeper than 500 km (Fig. 6.7). Baba et al. (2010) explained that conductivity increases to reach 3×10^{-2} S/m between 50 and 250–300 km depth and slightly decreases at deeper parts of the upper mantle, under

the Pacific Ocean to the east of the Izu Islands. These two models show no high-conductivity layer at the top of the asthenosphere, but some high-conductivity regions at deeper levels.

In summary, the high-conductivity layers with a conductivity maximum exist at the top of the asthenosphere under relatively young plates, with associated conductivity anisotropy. Such layers do not exist at the top of the asthenosphere under mature plates, and high-conductivity regions without a clear maximum may exist in deeper regions (150–400 km depth).

The high-conductivity layers were often interpreted in view of the proton conduction of olivine (Karato 1990; Evans et al. 2005). However, Yoshino et al. (2006, 2009a, b) argued that the magnitudes of the proton conduction are not enough to explain the high-conductivity layers at the top of the asthenosphere, because of the limited water solubility in olivine at low pressures. The temperature at 100 km depth along the adiabatic geotherm is 1670 ± 20 K, and the olivine intrinsic conduction is 4×10^{-3} S/m. The maximum water content in the 3 GPa is 600 ppm, according to Mosenfelder et al. (2006), which gives a proton conduction of 4×10^{-3} S/m. Yoshino et al. (2006) also argued that the anisotropy of the proton conduction is negligibly small at temperatures corresponding to the top of the asthenosphere. Thus, the high-conductivity layers associated with conductivity anisotropy at the top of the asthenosphere cannot be explained by the proton conduction, although the magnitude of the high-conductivity layers can be explained using the data set from Wang et al. (2006).

Partial melting is an alternative interpretation of the high-conductivity layers. Although it is usually difficult to expect partial melting in regions deeper than 80 km in anhydrous peridotite, the trace amounts of volatiles, H_2O, and CO_2 should produce partial melting down to 180–200 km depth even in a DMM composition (Hirschmann 2010; Dasgupta et al. 2013). Sifre et al. (2014) argued that the high-conductivity layers should originate in trace partial melting induced by trace amounts of H_2O and CO_2. Sifre et al. (2014) assumed the H_2O and CO_2 contents of 200 and 100–500 ppm, respectively, for the DMM mantle and interpreted the high-conductivity layers. However, their assumed CO_2 contents are too high in comparison with the commonly accepted values (cf. Workman et al. 2006). Here, we have to estimate the bulk conductivity of peridotite with incipient melting due to 100 ppm of H_2O and 50 ppm of CO_2. The melt fraction at 100 km depth is about 0.1 wt%, according to Dasgupta et al. (2013). Sifre et al. (2014) analysis suggests that the CO_2 and H_2O contents in the 0.1 % partial melt should be 1.3 and 6.5 %, respectively, and its conductivity should be 3.2×10^{1} S/m. Therefore, the bulk conductivity would be 3×10^{-2} S/m. Therefore, the partial melting hypothesis is also insufficient to explain the high-conductivity layers near mid-oceanic ridges if we assume the above volatile contents in the DMM.

As mentioned above, the high-conductivity layer shows conductivity anisotropy (Evans et al. 2005; Baba et al. 2006a, b; Naif et al. 2013). Since conductivity anisotropies of intrinsic and proton conductions of olivine are both small, the anisotropy in the high-conductivity layer cannot be explained with the conductivity of olivine. On the other hand, Zhang et al. (2014) demonstrated that partially melted

peridotite can produce conductivity anisotropy between the normal and parallel to shear directions on a shear plane. Therefore, the presence of conductivity anisotropy implies the presence of partial melting in these regions. Since the magnitude of partially molten peridotite at the top of the asthenosphere with 100 and 50 ppm of H_2O and CO_2, respectively, is much lower than the observation, the actual volatile contents in the DMM could be higher than these values and might be 200 and 100–500 ppm, respectively, as Sifre et al. (2014) assumed.

6.3.4 *Vertical Conductivity Structure in the Deep Upper Mantle*

Xu et al. (1998) claimed a conductivity jump by more than one order of magnitude for the olivine–wadsleyite transition and essentially no jump for the wadsleyite and ringwoodite transition. Although smoothing conditions are included in building a conductivity model from MT data, these were not applied at a 400 km depth to create a conductivity jump for the olivine–wadsleyite transition in order to construct a large-scale model (Utada et al. 2003). The current experimental data, however, suggest no large conductivity jump associated with the olivine–wadsleyite transition in intrinsic conduction or even imply a decrease in conductivity for this transition. It seems that Xu et al. (1998) obtained the high conductivity of wadsleyite and ringwoodite due to proton conduction (Huang et al. 2005). The decrease in conductivity for the olivine–wadsleyite transition is due to the ionic conduction in olivine but not in wadsleyite. It is not clear whether the absence of ionic conduction in wadsleyite is due to the limited experimental technology in laboratory conductivity measurement (Fig. 6.9).

Figure 6.10 shows the most recent semi-global 1D conductivity models with and without the application of smoothing conditions at 400, 550, and 650 km depths under the northern Pacific Ocean reported by Shimizu et al. (2010a, b).

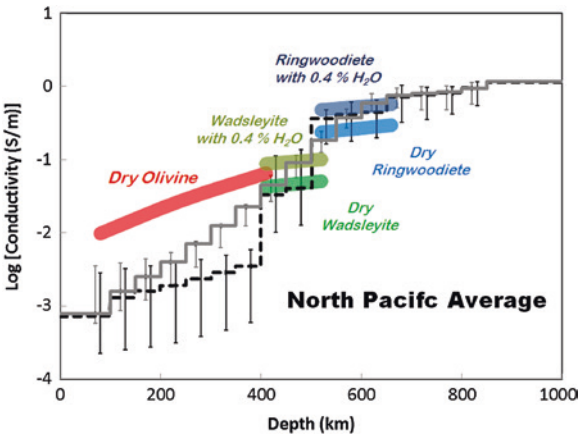

Fig. 6.9 The average one-dimensional conductivity structure under the North Pacific Ocean reported by Shimizu et al. (2010a). This model describes three conductivity jumps at 400, 500, and 650 km depths. The conductivities of wadsleyite and ringwoodite with 0 and 0.4 wt% of water are shown based on data by (Yoshino et al. (2008a, b, c)). The conductivity of dry olivine is also shown (Yoshino et al. 2009a, b)

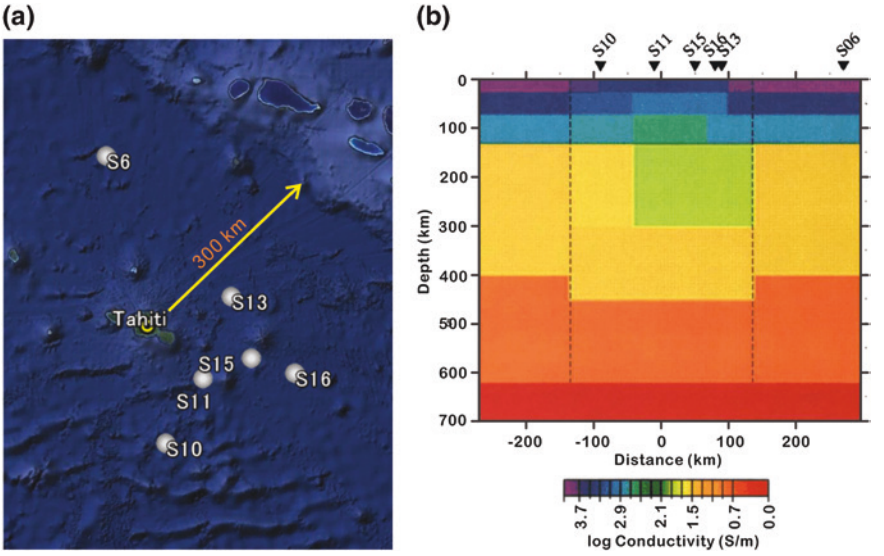

Fig. 6.10 The 2D conductivity structure near Tahiti (modified from Nolasco et al. 1998). **a** The locality of the observatories (labeled S6, S10, S1, S13, S15, and S16). The size of the Hawaiian plume, marked by an *arrow*, is 300 km (Montelli et al. 2006). **b** The two-dimensional conductivity structure approximately from NNW to SSE according to Nolasco et al. (1998). The locations of the observatories are marked on the figure. The conductivity is higher than the surrounding mantle in the region that is shallower than 130 km depth, whereas it is identical or even lower in the deeper regions

The conductivity of dry olivine, wadsleyite and ringwoodite, and wadsleyite and ringwoodite with 0.4 % of water is shown for comparison. The conductivity in the upper mantleabove 400 km in these models is significantly lower than that of intrinsic conduction in olivine. However, Shimizu et al. (2010a) used the long period range of MT signals (0.5–113 days), and therefore, the conductivity above 400 km depth was not well constrained (Baba et al. 2010). The conductivity in the transition zone in these models can be explained by intrinsic conduction in wadsleyite and ringwoodite. Because large amounts of water can be incorporated in these minerals, many attempts have been made to estimate water contents in the mantle transition zone by comparing the geophysical models and laboratory measurements (Huang et al. 2005; Yoshino et al. 2008a, b, c; Manthilake et al. 2009; Dai and Karato 2009; Romano et al. 2009; Yoshino and Katsura 2012). However, Fig. 6.10 demonstrates that the conductivity values of the transition zone depend on the modeling assumption. The uncertainty of each model is also large, and it is therefore found that estimation of the abundance of water in the transition zone in this way is not yet meaningful.

6.3.5 Local Conductivity Structures Under Hot Spots

Nolasco et al. (1998) studied conductivity structures under the Tahiti hot spot (Fig. 6.11). They showed about half an order of magnitude higher conductivity

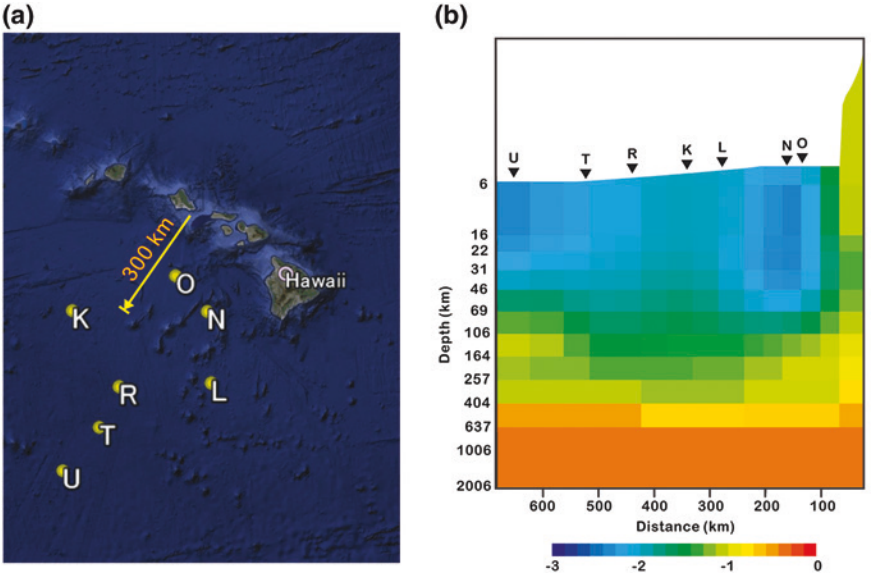

Fig. 6.11 The 2D conductivity structure southwest of Hawaii (modified from Constable and Heinson 2004). **a** The localities of observatories (labeled K, L, N, O, R, T, and U). The size of the Hawaiian plume, marked by an *arrow*, is 300 km (Montelli et al. 2006). **b** The two-dimensional conductivity structure approximately NE to SW, indicating the locations of observatories (Constable and Heinson 2004)

down to the depth of 130 km. However, deeper regions have equivalent or even lower conductivity than the surrounding regions. On the other hand, a seismic study shows clear, low-velocity anomalies from the depth of 300 km to the bottom of the mantle (Montelli et al. 2006). Constable and Heinson (2004) showed a two-dimensional conductivity model beneath the region southwest of Hawaii (Fig. 6.12). Their model also does not show conductivity anomalies in this region. Seismic tomography, however, shows a clear 1 % P-wave anomaly beneath Hawaii (Montelli et al. 2006).

The 1 % P-wave velocity anomaly would correspond to a temperature higher by 150 K. This temperature anomaly would increase the intrinsic conductivity of the main upper mantle minerals by half an order of magnitude. This high conductivity should be detectable by MT observations. In addition, geochemical studies show that sources of the ocean island basalt are enriched and have up to several factors higher volatile components (cf. Wallace 1998). As previously mentioned, high-volatile contents should always increase bulk conductivity by the proton conduction or melt network. For these reasons, the absence of high-conductivity zones under the hot spots cannot be explained consistently, based on available knowledge of mineral physics, seismology, and geochemistry.

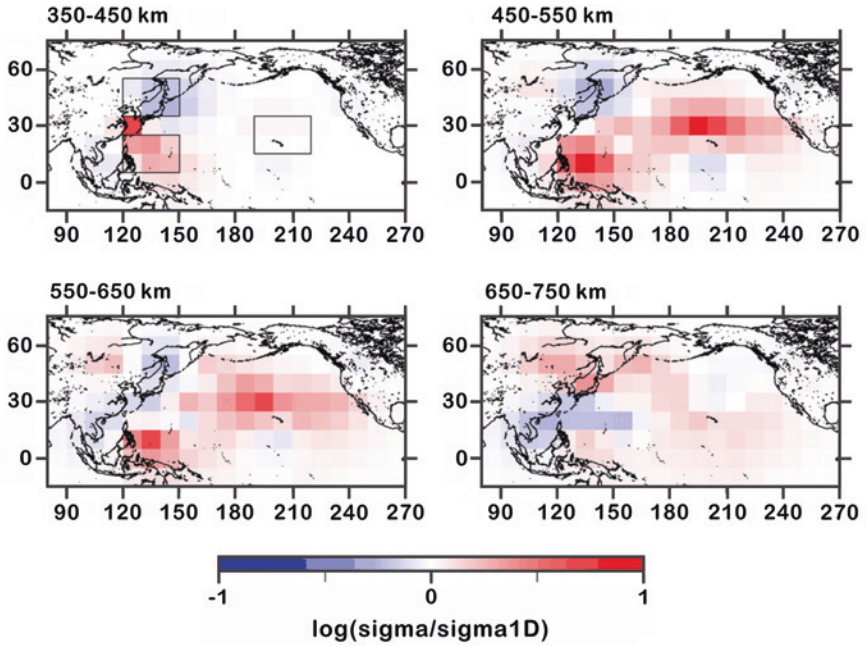

Fig. 6.12 Three-dimensional conductivity structure under the Pacific Ocean (modified from Shimizu et al. 2010b). The strong high-conductivity anomaly (*red*) is visible under the southern Philippine Sea. Another weak and broad high-conductivity anomaly is visible in the north of Hawaii

6.3.6 Conductivity Anomalies in the Transition Zone

Shimizu et al. (2010b) report a 3D conductivity structure from a depth of 350–850 km beneath the Pacific Ocean. They show a strong high-conductivity anomaly in the mantle transition zone under the southern Philippine Sea (Fig. 6.11). The center of the high-conductivity anomaly is located from the West Philippine Basin to the Caroline Basin. In contrast, the northern part of the Philippine Sea shows no conductivity anomaly. The maximum magnitude of high conductivity is about 0.8 log unit. The center of the high-conductivity anomaly is located at a depth of 450–550 km, becoming weaker at a depth of 550–650 km depth and turning into a low-conductivity anomaly in the top part of the lower mantle.

It is possible that this high-conductivity anomaly is caused by high-volatile contents in the region. If this high-conductivity anomaly was caused by the proton conduction of wadsleyite, the water contents in this region would be found to be 0.5 wt% in the upper part of the transition zone. Since wadsleyite

and ringwoodite can contain water more than 2 wt% (Keppler and Bolfan-Casanova 2006), the amount of 0.5 wt% water in wadsleyite is possible. It is noteworthy that the petrological study on Mariana back-arc trough magma (Stolper and Newman 1994) suggests such high water content in these regions. Another explanation for this is partial melting. However, the enhancement of bulk conductivity by partial melting has not been studied under the conditions of the mantle transition zone, and we therefore cannot argue this possibility at present.

Although the high-conductivity anomaly can be explained by assuming larger amounts of volatile components, the possible high-volatile contents in the upper part of the mantle transition zone under the southern part of the Philippine Sea are difficult to explain. Although there are complex subduction systems in this region, the high-conductivity anomaly in this region should not be directly attributed to the subduction of the Pacific plate to the Philippine Sea, because the high-conductivity anomaly does not exist in the northern part of the Philippine Sea. There is no reason for a drastic difference in transported water between the northern and southern parts of the Philippine Sea.

Shimizu et al. (2010b) also show a high-conductivity anomaly under the region north of Hawaii. The depth range of this anomaly is from 450 to 650 km. The east–west dimension of the high-conductivity region extends over 6000 km. The global seismic tomography shows a low-velocity anomaly beneath Hawaii. However, the low-velocity anomaly is located just below or even west of Hawaii. Consequently, high-conductivity and low-velocity anomalies are not caused by the same mechanism. The low-velocity anomaly is caused by a temperature anomaly, whereas the high-conductivity anomaly is caused by a compositional anomaly. This difference results in variation of a specific scale between these two anomalies. The very small dimension of high-temperature regions should be detected by P-wave tomography but would be too small for the analysis of the semi-global 3D structure of conductivity.

6.3.7 Fine-Scale Conductivity Variation Under the Philippine Sea

As previously explained, the semi-global 3D structures in conductivity show the high-conductivity anomaly in the upper part of the mantle transition zone under the south Philippine Sea. In addition to this, a regional study shows other anomalous features under the Philippine Sea (Seama et al. 2007). The study comprised a two-dimensional conductivity structure (Fig. 6.12b) from the south of the Mariana Trough to the north of the Daito Ridge (under the yellow line in Fig. 6.12a). This showed a strong high-conductivity anomaly exceeding 1×10^{-1} S/m under one

point east of the Ryukyu-Palau ridge between the Shikoku and Parece Vela basins (Point 4 in Fig. 6.12a) and weaker but still strong anomalies west of the northern part of the Ryukyu-Palau Ridge (Points 5 and 6). The peaks of these high-conductivity anomalies are located at a depth of 50–150 km. In contrast to these high-conductivity anomalies, the study found no high-conductivity anomaly under the Mariana Trough. Matsuno et al. (2010) also reported an absence of high-conductivity anomalies beneath the Mariana Trough (under the pink line in Fig. 6.12a).

The regions in which the high-conductivity anomalies are found were active in the past (40–60 million years ago). The region of no conductivity anomalies is located in the currently active volcanic zone. A seismic study shows a very strong S-wave velocity anomaly up to −8 % in this region (Isse et al. 2009) (Fig. 6.12c). It also shows that the low-velocity anomaly becomes weaker and deeper with increasing plate age from 0 to 100 million years. Actually, the region that shows the strongest S-wave velocity anomaly is under the Mariana Trough. The 8 % S-wave anomaly may indicate a temperature anomaly of 200 K, if we attribute the S-wave anomaly to a temperature anomaly only. This temperature anomaly should raise conductivity by 0.6 orders of magnitude, assuming a base temperature of 1660 K at 80 km depth. Thus, the absence of a high-conductivity layer is contrary to our expectation from the tectonic setting and seismic observation.

One possible explanation is that while volatile components or melts are successively supplied from the deeper part of the mantle to the upper mantle, the currently active zone has been releasing the volatile components. As a result, the non-active regions become volatile rich, whereas the active region becomes volatile poor. However, we note that the maximum water content at 100 km depth is only 500 ppm (cf. Keppler and Bolfan-Casanova 2006). The magnitude of proton conduction by this amount of water is negligible in comparison with the intrinsic conduction. The high-conductivity anomaly could be explained by the presence of partial melt. The Mariana Trough basalt contains 2 % of water (Stolper and Newman 1994), which suggests melt conductivity of 10 S/m. Therefore, the conductivity anomaly exceeding 1×10^{-1} S/m should indicate a melt fraction more than 1 %, which should cause some degree of low shear-wave anomaly. Actually, Isse et al. (2009) showed some low shear-wave anomaly under the Points 4, 5, and 6 in the Seama et al. (2007) study. This hypothesis could thus explain the high-conductivity anomaly under the Kyushu-Palau Ridge. There is yet no persuasive explanation for the low-conductivity anomaly under the Mariana Trough (Fig. 6.13).

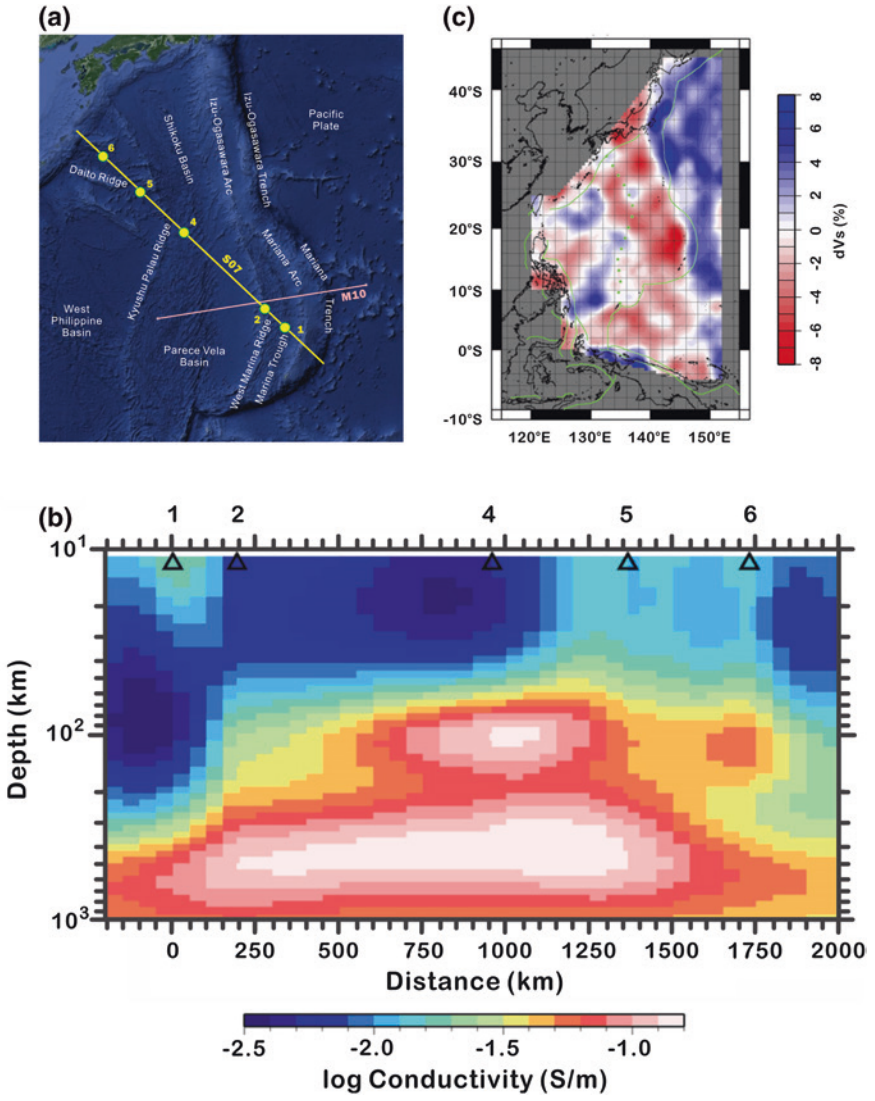

Fig. 6.13 Comparison of conductivity and seismic anomalies under the Philippine Sea. **a** Location of the observation sites in Seama et al. (2007). **b** 2D conductivity structure along the observation line S07 shown in **a**. The region under the Mariana Trough (OBEM1) at 40–200 km depth has low conductivity (modified from Seama et al. 2007). **c** The shear-wave anomaly under the Philippine Sea at 80 km depth (Isse et al. 2009). The region under the Mariana Trough has the low shear-wave anomaly, suggesting high temperatures (modified from Isse et al. 2009)

6.4 Concluding Remarks

We have reviewed the results of laboratory experiments about the conductivity of upper mantle minerals and representative MT observations under oceans. Conductivity in the upper mantle varies by more than three orders of magnitude. We have the following qualitative explanation for the following results obtained by the MT method.

1. The high conductivity just below the mid-oceanic ridges is mainly due to partial melting and partly due to high temperature.
2. The very low conductivity in the lithosphere is due to low temperatures.
3. The gradually increasing conductivity in the asthenosphere is due to the temperature increases in the adiabatic geotherm.
4. The high-conductivity layers are a feature of the asthenosphere under young plates. They associate conductivity anisotropy, which implies its partial melting origin.
5. There should be no large conductivity jump at the 410 km depth.
6. The high-conductivity anomaly in the mantle transition zone under the south of the Philippine Sea may be due to high water content.
7. The high-conductivity anomaly in the mantle transition zone north of Hawaii may be due to the volatile components of plume source.

The mantle structures under oceans are expected to be simpler than those under continents. Therefore, we expect that we can obtain quantitative and robust explanations. Nevertheless, the above explanations have the following serious problems.

1. The conductivity in the uppermost part of the lithosphere is too high by far, considering its low temperatures based on the ocean floor cooling model.
2. The magnitude of the high-conductivity layers at the top of the asthenosphere is difficult to explain based on the usually assumed volatile contents in the DMM.
3. The high-temperature anomalies inferred from the seismic tomography indicate no or little effect on the conductivity structures.
4. The local conductivity anomalies disagree with those expected from the tectonic setting.
5. In general, the conductivity in the upper mantle is higher than that expected from the experimental results.

Acknowledgement The author acknowledges S. Baba and T. Kogiso for their helpful discussion.

References

Angell CA, Smith DL (1982) Test of the entropy basis of the vogel-tammann-fulcher equation—dielectric-relaxation of polyalcohols near tg. J Phys Chem 86(19):3845–3852

Baba K (2005) Electrical structure in marine tectonic settings. Surv Geophys 26(6):701–731

Baba K, Chave AD, Evans RL, Hirth G, Mackie RL (2006a) Mantle dynamics beneath the East Pacific Rise at 17 degrees S: Insights from the Mantle Electromagnetic and Tomography (MELT) experiment. J Geophys Res-Solid Earth 111(B2). doi:10.1029/2004JB003598

Baba K, Tarits P, Chave AD, Evans RL, Hirth G, Mackie RL (2006b) Electrical structure beneath the northern MELT line on the East Pacific Rise at 15° 45′S. Geophys Res Lett 33(22). doi:10.1029/2006gl027528

Baba K, Utada H, Goto T, Kasaya T, Shimizu H, Tada N (2010) Electrical conductivity imaging of the Philippine Sea upper mantle using seafloor magnetotelluric data. Phys Earth Planet Inter 183(1–2):44–62

Caricchi L, Gaillard F, Mecklenburgh J, Trong EL (2011) Experimental determination of electrical conductivity during deformation of melt-bearing olivine aggregates: implications for electrical anisotropy in the oceanic low velocity zone. Earth Planet Sci Lett 302(1–2):81–94. doi:10.1016/j.epsl.2010.11.041

Constable S (1993) Conduction by mantle hydrogen. Nature 362(6422):704

Constable S (2006) SEO3: a new model of olivine electrical conductivity. Geophys J Int 166(1):435–437

Constable S, Duba A (1990) Electrical conductivity of olivine, a dunite, and the mantle. J Geophys Res 95(B5):6967–6978

Constable S, Heinson G (2004) Hawaiian hot-spot swell structure from seafloor MT sounding. Tectonophysics 389(1–2):111–124

Constable S, Shankland TJ, Duba A (1992) The electrical conductivity of an isotropic olivine mantle. J Geophys Res 97(B3):3397–3404

Constable SC, Heinson GS, Anderson G, White A (1997) Seafloor electromagnetic measurements above axial seamount, juan de fuca ridge. J Geomagn Geoelectr 49(11–12):1327–1342

Dai L, Karato SI (2009) Electrical conductivity of wadsleyite at high temperatures and high pressures. Earth Planet Sci Lett 287:277–283

Dasgupta R, Mallik A, Tsuno K, Withers AC, Hirth G, Hirschmann MM (2013) Carbon-dioxide-rich silicate melt in the Earth's upper mantle. Nature 493(7431):211–215. doi:10.1038/nature11731

Du Frane WL, Roberts JJ, Toffelmier DA, Tyburczy JA (2005) Anisotropy of electrical conductivity in dry olivine. Geophys Res Lett 32(24):L24315

Duba A, Constable S (1993) The electrical conductivity of lherzolite. J Geophys Res Solid Earth 98(B7):11885–11899

Evans RL et al (1999) Asymmetric electrical structure in the mantle beneath the East Pacific rise at 17° S. Science 286(5440):752–756 (Artn l24315)

Evans RL, Hirth G, Baba K, Forsyth D, Chave A, Mackie R (2005) Geophysical evidence from the MELT area for compositional controls on oceanic plates. Nature 437(7056):249–252

Faul UH (1997) Permeability of partially molten upper mantle rocks from experiments and percolation theory. J Geophys Res-Solid Earth 102(B5):10299–10311. doi:10.1029/96jb03460

Filloux JH (1977) Ocean-floor magnetotelluric sounding over north-central Pacific. Nature 269:297–301

Forsyth DW et al (1998) Imaging the deep seismic structure beneath a mid-ocean ridge: the MELT experiment. Science 280(5367):1215–1218

Fuji-ta K, Katsura T, Tainosho Y (2004) Electrical conductivity measurement of granulite under mid- to lower crustal pressure-temperature conditions. Geophys J Int 157:79–86

Fuji-ta K, Katsura T, Matsuzaki T, Ichiki M, Kobayashi T (2007) Electrical conductivity measurement of gneiss under mid- to lower crustal P-T conditions. Tectonophysics 434:93–101

Fukao Y, Koyama T, Obayashi M, Utada H (2004) Trans-Pacific temperature field in the mantle transition region derived from seismic and electromagnetic tomography. Earth Planet Sci Lett 217(3–4):425–434

Gaillard F (2004) Laboratory measurements of electrical conductivity of hydrous and dry silicic melts under pressure. Earth Planet Sci Lett 218(1–2):215–228

Gaillard F, Malki M, Iacono-Marziano G, Pichavant M, Scaillet B (2008) Carbonatite melts and electrical conductivity in the asthenosphere. Science 322(5906):1363–1365

Heinson G, Constable SH (1992) The electrical conductivity of the oceanic upper mantle. Geophys J Int 110(1):159–179

Heinson GS, Lilley FEM (1993) An application of thin-sheet electromagnetic modelling to the Tasman Sea. Phys Earth Planet Inter 81(1–4):231–251
Heinson GS, White A, Law LK, Hamano Y, Utada H, Yukutake T, Segawa J, Toh H (1993) EMRIDGE: the electromagnetic investigation of the Juan de Fuca Ridge. Mar Geophys Res 15(2):77–100. doi:10.1007/bf01204130
Heinson G, Constable S, White A (1996) Seafloor magnetotelluric sounding above axial seamount. Geophys Res Lett 23(17):2275–2278
Heinson G, Constable S, White A (2000) Episodic melt transport at mid-ocean ridges inferred from magnetotelluric sounding. Geophys Res Lett 27(15):2317–2320
Hirschmann MM (2010) Partial melt in the oceanic low velocity zone. Phys Earth Planet Inter 179(1–2):60–71
Huang XG, Xu YS, Karato SI (2005) Water content in the transition zone from electrical conductivity of wadsleyite and ringwoodite. Nature 434:746–749
Hung SH, Shen Y, Chiao LY (2004) Imaging seismic velocity structure beneath the Iceland hot spot: a finite frequency approach. J Geophys Res-Solid Earth 109(B8), B08305. doi: 10.1029/2003jb002889
Isse T et al (2009) Seismic structure of the upper mantle beneath the Philippine Sea from seafloor and land observation: Implications for mantle convection and magma genesis in the Izu-Bonin-Mariana subduction zone. Earth Planet Sci Lett 278(1–2):107–119
Jacobsen SD (2006) Effect of water on the equation of state of nominally anhydrous minerals. In: Keppler H, Smith JR (eds) Water in nominally anhydrous minerals. Geochemical Society, Mineralogical Society of America, USA, pp 321–342
Jones AG, Evans RL, Eaton DW (2009) Velocity-conductivity relationships for mantle mineral assemblages in Archean cratonic lithosphere based on a review of laboratory data and Hashin-Shtrikman extremal bounds. Lithos 109(1–2):131–143. doi:10.1016/j.lithos.2008.10.014
Karato S (1990) The role of hydrogen in the electrical conductivity of the upper mantle. Nature 347(6290):272–273
Karato S, Dai LD (2009) Comments on "Electrical conductivity of wadsleyite as a function of temperature and water content" by Manthilake et al. Phys Earth Planet Inter 174:19–21
Katsura T, Sato K, Ito E (1998) Electrical conductivity of silicate perovskite at lower-mantle conditions. Nature 395:493–495
Katsura T, Yokoshi S, Kawabe K, Shatskiy A, Okube M, Fukui H, Ito E, Nozawa A, Funakoshi K-I (2007) Pressure dependence of electrical conductivity of (Mg, Fe)SiO3 ilmenite. Phys Chem Miner 34:249–255
Katsura T, Yoneda A, Yamazaki D, Yoshino T, Ito E (2010) Adiabatic temperature profile in the mantle.Phys. Earth Planet. Inter., 183(1–2):212–218. doi:10.1016/j.pepi.2010.07.001
Keppler H, Bolfan-Casanova N (2006) Thermodynamics of water solubility and partitioning. In: Keppler H, Smith JR (eds) Water in nominally anhydrous minerals. Geochemical Society, Mineralogical Society of America, USA, pp 193–230
Key K, Constable S, Liu LJ, Pommier A (2013) Electrical image of passive mantle upwelling beneath the northern East Pacific Rise. Nature 495(7442):499–502. doi:10.1038/nature11932
Kohlstedt DL, Mackwell SJ (1998) Diffusion of hydrogen and intrinsic point defects in olivine. Zeitschrift Fur Physikalische Chemie-Int J Res Phys Chem Chem Phys 207:147–162
Larsen JC (1975) Low-frequency (0.1-6.0 CPD) Electromagnetic study of deep mantle electrical-conductivity beneath Hawaiian-Islands. Geophys J Roy Astron Soc 43(1):17–46
Lizarralde D, Chave A, Hirth G, Schultz A (1995) Northeastern pacific mantle conductivity profile from long-period magnetotelluric sounding using Hawaii-to-California submarine cable data. J Geophys Res-Solid Earth 100(B9):17837–17854
Mackwell SJ, Kohlstedt DL (1990) Diffusion of hydrogen in olivine: implications for water in the mantle. J Geophys Res 95(B4):5079–5088
Manthilake M, Matsuzaki T, Yoshino T, Yamashita S, Ito E, Katsura T (2009) Electrical conductivity of wadsleyite as a function of temperature and water content. Phys Earth Planet Inter 174(1–4):10–18. doi:10.1016/j.pepi.2008.06.001

Matsuno T et al (2010) Upper mantle electrical resistivity structure beneath the central Mariana subduction system. Geochem Geophys Geosyst 11:Q09003

Mibe K, Kawamoto T, Matsukage KN, Fei Y, Ono S (2011) Slab melting versus slab dehydration in subduction-zone magmatism. Proc Natl Acad Sci USA 108(20):8177–8182

Montelli R, Nolet G, Dahlen FA, Masters G (2006) A catalogue of deep mantle plumes: New results from finite-frequency tomography. Geochem Geophys Geosyst 7(11):Q11007

Mosenfelder JL, Deligne NI, Asimow PD, Rossman GR (2006) Hydrogen incorporation in olivine from 2-12 GPa. Am Miner 91(2–3):285–294. doi:10.2138/am.2006.1943

Naif S, Key K, Constable S, Evans RL (2013) Melt-rich channel observed at the lithosphereasthenosphereboundary. Nature 495(7441):356–359. doi:10.1038/nature11939

Ni HW, Keppler H, Behrens H (2011) Electrical conductivity of hydrous basaltic melts: implications for partial melting in the upper mantle. Contrib Mineral Petrol 162(3):637–650

Nichols ARL, Carroll MR, Hoskuldsson A (2002) Is the Iceland hot spot also wet? Evidence from the water contents of undegassed submarine and subglacial pillow basalts. Earth Planet Sci Lett 202(1):77–87. doi:10.1016/s0012-821x(02)00758-6

Nolasco R, Tarits P, Filloux JH, Chave AD (1998) Magnetotelluric imaging of the Society Islands hotspot. J Geophys Res-Solid Earth 103(B12):30287–30309

Ohta K, Hirose K, Ichiki M, Shimizu K, Sata N, Ohishi Y (2010) Electrical conductivities of pyrolitic mantle and MORB materials up to the lowermost mantle conditions. Earth Planet Sci Lett 289(3–4):497–502

Oldenburg DW (1981) Conductivity structure of oceanic upper mantle beneath the Pacific plate. Geophys J Royal Astron Soc 65:359–394

Omura K, Kurita K, Kumazawa M (1989) Experimental study of pressure dependence of electrical conductivity of olivine at high temperatures. Phys Earth Planet Inter 57(3–4):291–303

Poe BT, Romano C, Nestola F, Smyth JR (2010) Electrical conductivity anisotropy of dry and hydrous olivine at 8 GPa. Phys Earth Planet Inter 181(3–4):103–111

Romano C, Poe BT, Tyburczy J, Nestola F (2009) Electrical conductivity of hydrous wadsleyite. Eur J Mineral 21:615–622

Schock RN, Duba AG, Shankland TJ (1989) Electrical-conduction in olivine. J Geophys Res-Solid Earth Planet 94(B5):5829–5839

Seama N, Baba K, Utada H, Toh H, Tada N, Ichiki M, Matsuno T (2007) 1-D electrical conductivity structure beneath the Philippine Sea: results from an ocean bottom magnetotelluric survey. Phys Earth Planet Inter 162(1–2):2–12

Shankland TJ, Duba AG (1990) Standard electrical conductivity of isotropic, homogeneous olivine in the temperature range 1200°–1500°C. Geophys J Int 103:25–31

Shimizu H, Koyama T, Baba K, Utada H (2010a) Revised 1-D mantle electrical conductivity structure beneath the north Pacific. Geophys J Int 180(3):1030–1048

Shimizu H, Utada H, Baba K, Koyama T, Obayashi M, Fukao Y (2010b) Three-dimensional imaging of electrical conductivity in the mantle transition zone beneath the North Pacific Ocean by a semi-global induction study. Phys Earth Planet Inter 183(1–2):252–269

Shimojuku A, Yoshino T, Yamazaki D (2014) Electrical conductivity of brine-bearing quartzite at 1 GPa: implications for fluid content and salinity of the crust. Earth Planet Space 66:9. doi:10.1186/1880-5981-66-2

Sifre D, Gardes E, Massuyeau M, Hashim L, Hier-Majumder S, Gaillard F (2014) Electrical conductivity during incipient melting in the oceanic low-velocity zone. Nature 509(7498):81–85. doi:10.1038/nature13245

Sinha MC, Navin DA, Macgregor LM, Constable S, Peirce C, White A, Heinson G, Inglis MA (1997) Evidence for accumulated melt beneath the slow-spreading Mid-Atlantic Ridge. Philos Trans R Soc A Math Phys Eng Sci 355(1723):233–253

Sobolev AV, Chaussidon M (1996) H_2O concentrations in primary melts from suprasubduction zones and mid-ocean ridges: implications for water storage and recycling in the mantle. Earth Planet Sci Lett 137:45–55

Stolper E, Newman S (1994) The role of water in the petrogenesis of Mariana trough magmas. Earth Planet Sci Lett 121(3–4):293–325

Tyburczy JA, Waff HS (1983) Electrical conductivity of molten basalt and andesite to 25 kilobars pressure: geophysical significance and implications for charge transport and melt structure. J Geophys Res 88(B3):2413–2430

Utada H, Koyama T, Shimizu H, Chave AD (2003) A semi-global reference model for electrical conductivity in the mid-mantle beneath the north Pacific region. Geophys Res Lett 30(4), 1194. doi:10.1029/2002GL016092

Velimsky J (2010) Electrical conductivity in the lower mantle: constraints from CHAMP satellite data by time-domain EM induction modelling. Phys Earth Planet Inter 180(3–4):111–117

Waff HS, Bulau JR (1979) Equilibrium fluid distribution in an ultramafic partial melt under hydrostatic stress conditions. J Geophys Res 84(NB11):6109–6114

Wallace PJ (1998) Water and partial melting in mantle plumes: Inferences from the dissolved H2O concentrations of Hawaiian basaltic magmas. Geophys Res Lett 25(19):3639–3642. doi:10.1029/98gl02805

Wanamaker BJ, Duba AG (1993) Electrical conductivity of San Carlos olivine along [100] under oxygen- and pyroxene-buffered conditions and implications for defect equilibria. J Geophys Res 98(B1):489–500

Wang D-J, Mookherjee M, Xu YS, Karato S (2006) The effect of water on the electrical conductivity of olivine. Nature 443(7114):977–980

Workman RK, Hauri E, Hart SR, Wang J, Blusztajn J (2006) Volatile and trace elements in basaltic glasses from Samoa: implications for water distribution in the mantle. Earth Planet Sci Lett 241(3–4):932–951. doi:10.1016/j.epsl.2005.10.028

Xu Y-S, Poe BT, Shankland TJ, Rubie DC (1998) Electrical conductivity of olivine, wadsleyite, and ringwoodite under upper-mantle conditions. Science 280(5368):1415–1418

Yang X-Z (2012) Orientation-related electrical conductivity of hydrous olivine, clinopyroxene and plagioclase and implications for the structure of the lower continental crust and uppermost mantle. Earth Planet Sci Lett 317:241–250

Yoshino T, Katsura T (2009) Effect of iron content on electrical conductivity of ringwoodite, with implications for electrical structure in the transition zone. Phys Earth Planet Inter 174(1–4):3–9

Yoshino T, Katsura T (2012) Re-evaluation of electrical conductivity of anhydrous and hydrous wadsleyite. Earth Planet Sci Lett 337:56–67

Yoshino T, Katsura T (2013) Electrical conductivity of mantle minerals: role of water in conductivity anomalies. In: Jeanloz R (ed) Annual review of earth and planetary sciences, vol 41. Annual Reviews, Palo Alto, p 605

Yoshino T, Walter MJ, Katsura T (2003) Core formation in planetesimals triggered by permeable flow. Nature 422:154–157

Yoshino T, Walter MJ, Katsura T (2004) Connectivity of molten Fe alloy in peridotite based on in situ electrical conductivity measurements: implications for core formation in terrestrial planets. Earth Planet Sci Lett 222:625–643

Yoshino T, Matsuzaki T, Yamashita S, Katsura T (2006) Hydrous olivine unable to account for conductivity anomaly at the top of the asthenosphere. Nature 443(7114):973–976

Yoshino T, Manthilake G, Matsuzaki T, Katsura T (2008a) Dry mantle transition zone inferred from the conductivity of wadsleyite and ringwoodite. Nature 451:326–329

Yoshino T, Nishi M, Matsuzaki T, Yamazaki D, Katsura T (2008b) Electrical conductivity of majorite garnet and its implications for electrical structure in the mantle transition zone. Phys Earth Planet Inter 170:193–200

Yoshino T, Yamazaki D, Ito E, Katsura T (2008c) No interconnection of ferro-periclase in post-spinel phase inferred from conductivity measurement. Geophys Res Lett 35:5

Yoshino T, Matsuzaki T, Shatskiy A, Katsura T (2009a) The effect of water on the electrical conductivity of olivine aggregates and its implications for the electrical structure of the upper mantle. Earth Planet Sci Lett 288(1–2):291–300

Yoshino T, Yamazaki D, Mibe K (2009b) Well-wetted olivine grain boundaries in partially molten peridotite in the asthenosphere. Earth Planet Sci Lett 283(1–4):167–173

Yoshino T, Laumonier M, McIsaac E, Katsura T (2010) Electrical conductivity of basaltic and carbonatite melt-bearing peridotites at high pressures: Implications for melt distribution and melt fraction in the upper mantle. Earth Planet Sci Lett 295(3–4):593–602. doi:10.1016/j.epsl.2010.04.050

Yoshino T, Ito E, Katsura T, Yamazaki D, Shan SM, Guo XZ, Nishi M, Higo Y, Funakoshi K (2011) Effect of iron content on electrical conductivity of ferropericlase with implications for the spin transition pressure. J Geophys Res-Solid Earth 116, B04202. doi:10.1029/2010jb007801

Yoshino T, McIsaac E, Laumonier M, Katsura T (2012a) Electrical conductivity of partial molten carbonate peridotite. Phys Earth Planet Inter 194:1–9

Yoshino T, Shimojuku A, Shan S-M, Guo X-Z, Yamazaki D, Ito E, Higo Y, Funakoshi K (2012b) Effect of temperature, pressure and iron content on the electrical conductivity of olivine and its high-pressure polymorphs. J Geophys Res-Solid Earth 117, B08205. doi:10.1029/2011jb008774

Zhang BH, Yoshino T, Wu XP, Matsuzaki T, Shan SM, Katsura T (2012) Electrical conductivity of enstatite as a function of water content: Implications for the electrical structure in the upper mantle. Earth Planet Sci Lett 357:11–20

Zhang B-H, Yoshino T, Yamazakil D, Manthilake G, Katsura T (2014) Electrical in partially molten peridotite under shear deformation, Earth Planet Sci Lett 405:98–109